IPP-Report

Max-Planck-Institut für Plasmaphysik

F. Kin, G. Birkenmeier, T. Happel, J. Pinzon, P. Hennequin, U. Stroth, S.-I. Itoh, K. Itoh, S. Inagaki, T. Kobayashi, ASDEX Upgrade Team

Comparison between I-mode and I-phase bursts in ASDEX Upgrade

IPP 2018-07
April 2018

Comparison between I-mode and I-phase bursts in ASDEX Upgrade

[1]F.Kin, [2,3]G.Birkenmeier, [2]T.Happel, [2,3]J.Pinzon, [4]P.Hennequin, [2,3]U.Stroth, [5,6]S.-I.Itoh, [6,7]K.Itoh, [5,6]S.Inagaki, [7]T.Kobayashi and the ASDEX Upgrade-Team

[1]Interdisciplinary Graduate School of Engineering Sciences, Kyushu University, 6-1 Kasuga Koen, Kasuga, Fukuoka 816-8580, Japan
[2]Max Plank Institute for Plasma Physics, Boltzmannstr. 2, 85748 Garching, Germany
[3]Physik-Department E28, Technische Universität München, James-Franck-Str. 1, 85748 Garching, Germany
[4]Laboratoire de Physique des Plasmas, Ecole Polytechnique, 91128 Palaiseau, France
[5]Research Institute for Applied Mechanics, Kyushu University, 6-1 Kasuga Koen, Kasuga, Fukuoka 816-8580, Japan
[6]Research Center for Plasma Turbulence, Kyushu University, 6-1 Kasuga Koen, Kasuga, Fukuoka 816-8580, Japan
[7]National Institute for Fusion Science, Oroshi-cho, Toki 509-5292, Japan

E-mail: kin@riam.kyushu-u.ac.jp

Abstract. The properties of bursts, precursor modes and turbulence during I-phase and I-mode are investigated in ASDEX Upgrade plasmas. Doppler reflectometry detects density bursts in both modes. Similarities and differences of turbulence behavior, time scale and intermittency are discussed. One of the similarities is an existence of a precursor before the density bursts. The behavior of magnetic fluctuations and density fluctuations is different in both modes. The time scales of the density bursts and magnetic fluctuations are estimated. The result suggests that I-phase density bursts are more related to magnetic fluctuations.

1. Introduction

The I-mode is known as interesting confinement regime [1, 2], where only the heat transport is suppressed, like in H-mode, but not the particle transport. Due to these unique transport characteristics, it is useful to study the turbulence behavior in I-mode, which may affect on transport. Recent studies observed the existence of density bursts, which might be connected to particle transport [3, 4]. These bursts are observed by Doppler reflectometry, and they are connected to the weakly coherent mode (WCM), which is a fluctuation generally observed in I-mode plasmas. In I-phase, which is a phase between L-H transitions with dithering of quantities like densities and poloidal

flows [5], density bursts are also observed [6]. Therefore, it is interesting to compare density bursts in both modes, such as durations, rise/decay times and intermittency.

The behavior of fluctuations during the bursts is also important. The WCM and precursors, which are associated with the density bursts, are also observed in I-mode and I-phase, respectively [3, 7]. In addition, a low frequency mode is observed during the bursts at ASDEX Upgrade (AUG) in both I-mode and I-phase [6, 8]. It is considered as the geodesic acoustic mode (GAM). Transport by turbulence is strongly related to E $\times$ B shearing [9]. GAMs or Zonal Flows contribute to these E $\times$ B shearing effects [10]. Therefore, studying of these low frequency modes and turbulence behavior is a key to the transport barrier formation.

This paper reports on turbulence characters during the bursts for I-mode and I-phase discharges by using Doppler reflectometry. The paper is organized as follows. Section 2 describes typical I-mode and I-phase discharges in AUG. Density bursts, which are observed by Doppler reflectometry, are presented in section 3. In section 4, conditional averaging is carried out to quantify the bursts and other fluctuations. Time scale and intermittency of the bursts are also estimated. Finally, we summarize the findings in section 5.

2. Late I-mode and late I-phase

The I-mode is obtained when the power threshold for H-mode access is kept high, for example, in upper-single null configuration, which is an unfavorable magnetic configuration in the standard AUG configuration. A typical I-mode discharge is shown in figure 1. The plasma is mainly heated by neutral beam injection (NBI) as shown in Fig. 1(a). The toroidal magnetic field strength is $B_t = -2.5\,\mathrm{T}$ and the plasma current is $I_p = 1.0\,\mathrm{MA}$, respectively. At around 2.25 s, L to I-mode transition starts with increasing the H98 confinement factor [11]. After the transition, the edge electron temperature (Fig. 1(c)) increases, while electron density does not increase so much (Fig. 1(b)). This is an I-mode feature that only the heat transport is reduced while the particle transport stays almost constant. The power spectra of density fluctuations, which is observed by conventional reflectometry, is shown in Fig. 1(f)-(h). In the biginning of the I-mode, density fluctuations around 40 kHz is observed. Thereafter, density fluctuations around 100 kHz appear, and these modes are the WCM [12]. The WCM is stronger and frequency increases in I-mode and the H98 confinement factor is close to 1. Poloidal magnetic field fluctuations measured with Mirnov coils, which are located at above the plasma, also becomes intermittent (Fig. 1(e)). This phase, we call late I-mode. In this discharge, late I-mode lasts approximately from 2.40 s to 2.44 s.

In contrast to the I-mode, the I-phase is observed in favorable configuration at the H-mode transition. A typical I-phase discharge is shown in figure 2. The electron cyclotron heating system (ECH) is one of the main external heating power in this shot (Fig. 2(a)). The toroidal magnetic field and the plasma current are the same as in the

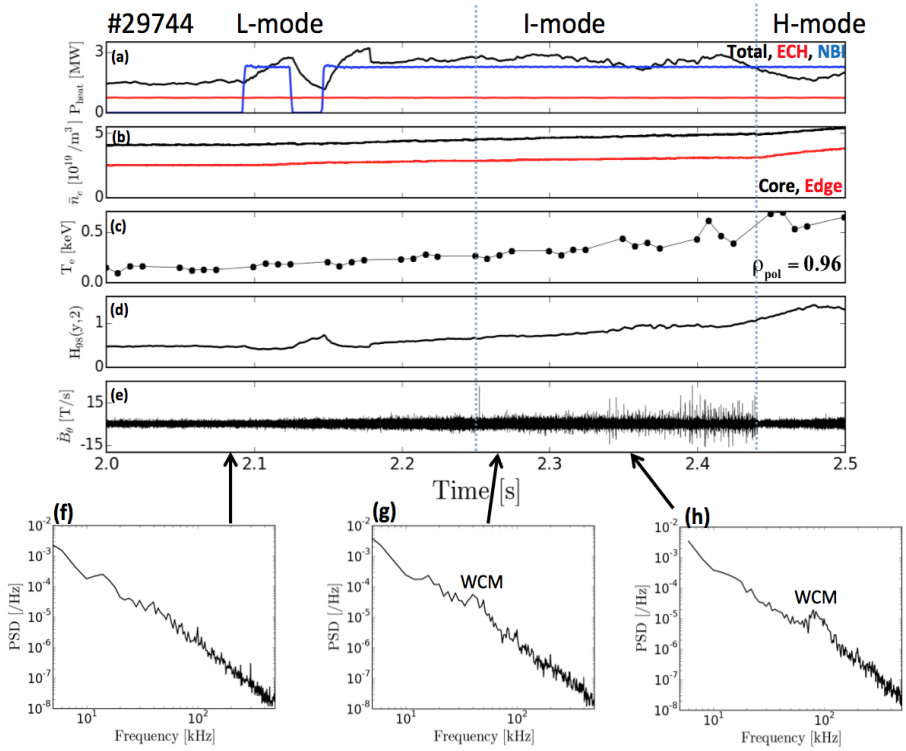

Figure 1. Time trace of a typical I-mode discharge showing (a) heating power, (b) line averaged density, (c) electron temperature measured by Thomson scattering, (d) confinement factor $H_{98}(y,2)$ and (e) poloidal magnetic field fluctuations (the coil name is C09-09). (f)-(h) Density fluctuation spectra measured by conventional reflectometry of the times indicated by the arrows.

I-mode discharge, and have a value of $B_t = -2.5\,\mathrm{T}$ and $I_p = 1.0\mathrm{MA}$, respectively. At around 3.52 s, the L to I-phase transition happens with an abrupt decrease of divertor current (Fig. 2(d)). The density and the electron temperature slightly increase during I-phase (Fig. 2(b) and (c)). The poloidal magnetic field fluctuations, which are measured below the divertor, oscillates after the L-I transition (Fig. 2(e)). However, the oscillation frequency decreases as shown in Fig. 2(g) and (h). Therefore, similar to I-mode, a late I-phase can also be defined. The I-phase is called late I-phase when the pedestal has developed. Sometimes, the bursts appear intermittently in this phase. In this discharge, the late I-phase starts at around 3.7 s and continues until around 4.4 s.

3. Density bursts

As it was shown above, the I-mode as well as the I-phase exhibits density bursts. In order to investigate the dynamics and turbulence behavior of these bursts, fast density measurments are needed. The main diagnostic used in this paper is the Doppler reflectometry system [13], which is applied here for measurments in the plasma edge region. Turbulence with perpendicular wavenumbers $k_\perp = 9 - 12\,\mathrm{cm}^{-1}$ were

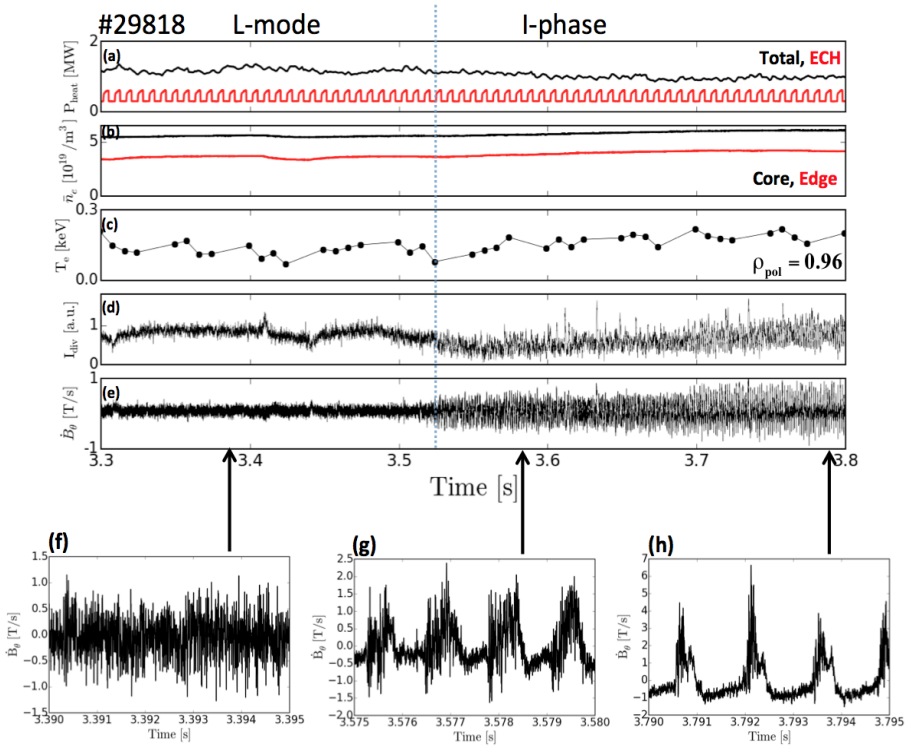

Figure 2. Time trace of a typical I-phase discharge showing (a) heating power, (b) line averaged density, (c) electron temperature measured by Thomson scattering, (d) divertor shunt current and (d) poloidal magnetic field fluctuations (the coil name is C09-23). (f)-(h) Time trace of the poloidal magnetic field fluctuations of the times indicated by the arrows.

detected. Figure 3(a),(b) and (d) show turbulence amplitudes measured with Doppler reflectometry in L-mode, late I-mode and late I-phase, respectively. Here the turbulence amplitude $S(t)$ is defined as $S(t) = \sqrt{I^2(t) + Q^2(t)}$, where $I(t)$ and $Q(t)$ indicate the real part and imaginary part of the Doppler reflectometer heterodyne signal. Compared to L-mode, strong density bursts appear intermittently in the late I-mode. In the late I-phase, density bursts appear concurrently with magnetic field dithering as shown in Fig. 3(c).

From figure 3(b) and (d), duration and intermittency of the bursts in late I-mode and late I-phase looks different, however, they have a similar character. Figure 4(a) and (b) show expanded density bursts in late I-mode and late I-phase, respectively. Before the main bursts, small turbulence bursts are seen periodically (hatched region in Fig. 4(a) and (b)). This occurs in different shots and might be precursors. The periods of the precursors are roughly 10 μs. Figure 4(c) and (d) indicate power spectra of conventional reflectometry signals in late I-mode and late I-phase, respectively. Around 100 kHz fluctuations are observed in both modes. In late I-mode, the 100 kHz fluctuations are the WCM, which frequency corresponds with the periods of the precursor. Fluctuations, which are closed to the WCM frequency, are observed in late I-phase.

Figure 5(a) and (c) show the power spectrum of the Doppler reflectometer

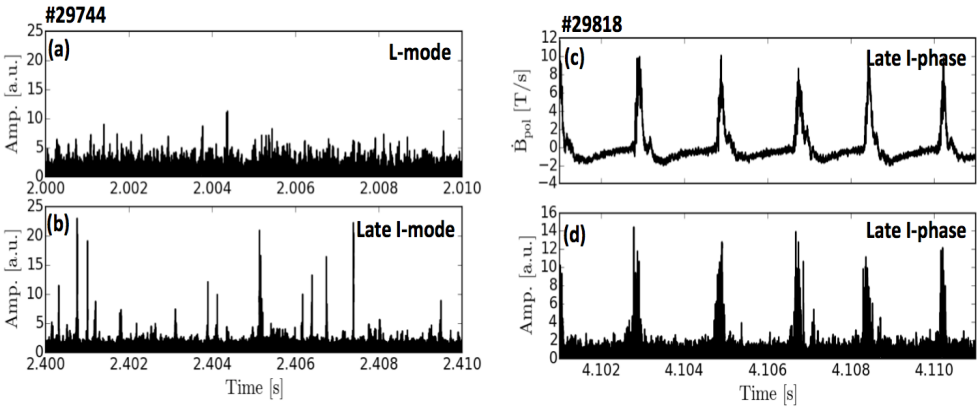

Figure 3. Time evolution of turbulence amplitude in (a) L-mode, (b) Late I-mode and (d) late I-phase. Bursts in the late I-phase are accompanied with (c) poloidal magnetic field fluctuations. (a) and (b) are the same discharge #29744 at different times. (c) and (d) are the same discharge #29818 at the same time.

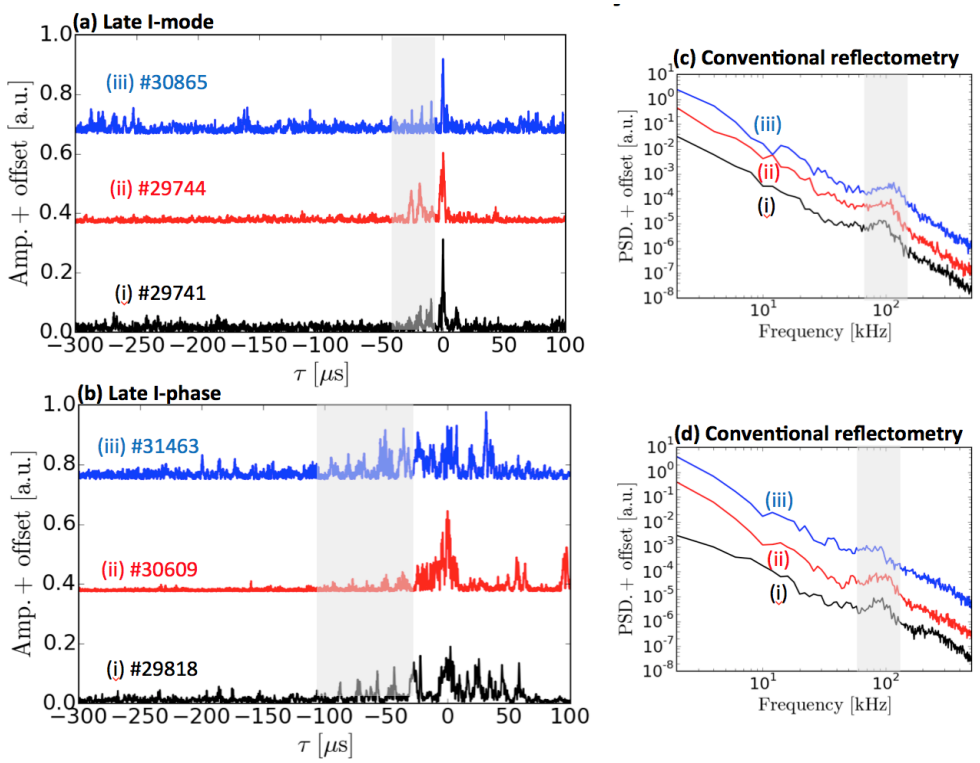

Figure 4. Examples of evolution of density bursts with different plasma discharges in (a) late I-mode and in (b) late I-phase. Density fluctuation power spectra in (c) late I-mode and in (d) late I-phase.

heterodyne signal in late I-mode and late I-phase, respectively. The spectra are calculated from data acquired in discharge #30865 (t = 3.8885-3.8887 s) and #29818 (t = 4.0191-4.0193 s) for late I-mode and late I-phase, respectively. A Doppler shift is observed in both modes and the peak in the spectrum is modulated. The zoom of the Doppler peaks in linear scale with Gaussian fits are shown in Fig. 5(b) and (d).

The Doppler peaks are clearly modulated with a frequency of around 100 kHz in late I-mode and of around 80 kHz in late I-phase, which almost coincide with conventional reflectometry spectra peak frequencies. This may be due to the modulation of turbulence amplitude measured by Doppler reflectometry. These results suggest the existence of a precursor before the bursts both in late I-mode and late I-phase.

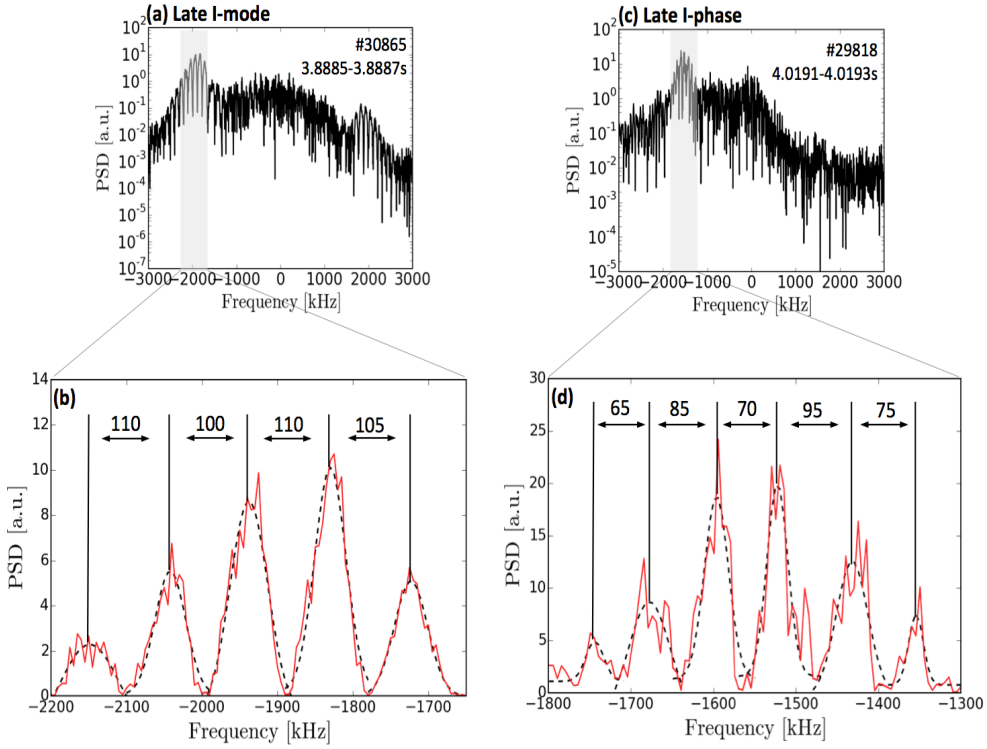

Figure 5. Power spectra of Doppler reflectometer heterodyne signal in (a) late I-mode and (c) late I-phase. Zoom into the Doppler peaks with Gaussian fits (black dashed line) in (b) and (d).

4. Conditional averaging

For quantifying turbulence during the bursts, conditional averaging [14] is applied. For late I-mode, density bursts, which are above a factor of 5 from standard deviation of the Doppler amplitude signal, are conditional averaged [8]. 78 events are obtained during 2.40-2.44 s of discharge #29744. Figure 6(a) and (f) show conditionally averaged density bursts. Conditionally averaged poloidal and radial magnetic field fluctuations are shown in (b) and (d), and their wavelet spectra are also shown in (c) and (e), respectively. Fluctuations around 100 kHz are confirmed, as shown in Fig. 6(c). This is most probably the geodesic Alfvenic mode (GAlf), as described in ref. [12]. The GAlf stationary exists, however, its increase during the bursts. The GAlf is also detected in radial magnetic field fluctuations during the bursts, as shown in Fig. 6(e). Figures

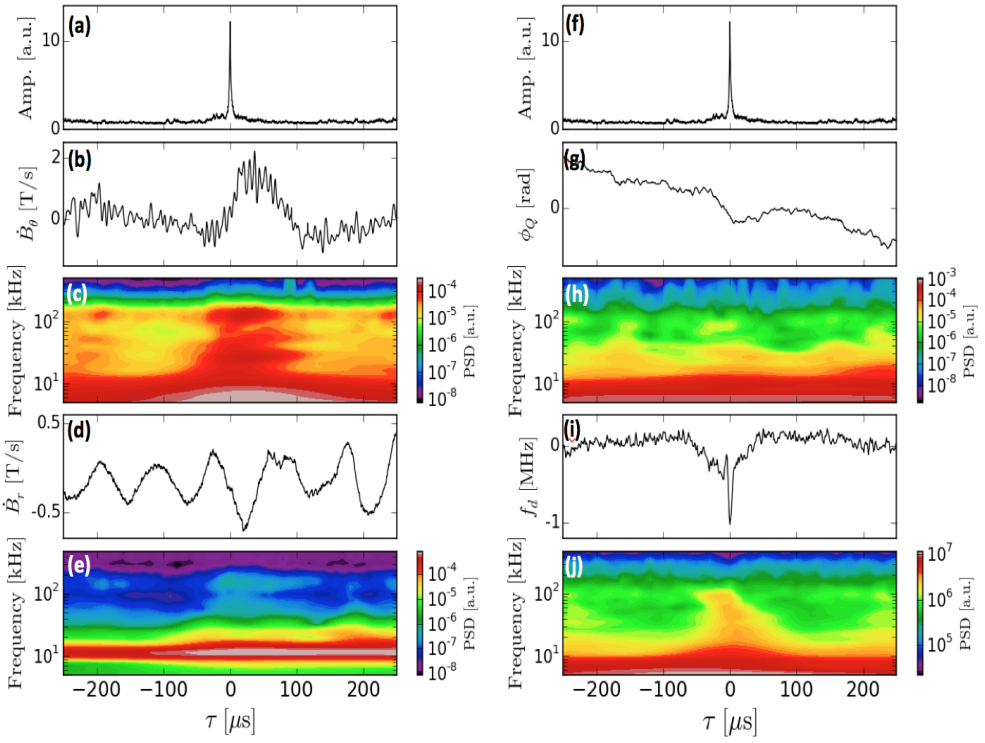

Figure 6. Dynamics of conditional averaged signals and their wavelet spectra in late I-mode. (a) and (f) show density bursts, (b) and (c) show poloidal magnetic field fluctuations and its spectrum, (d) and (e) show radial magnetic field fluctuations and its spectrum, (g) and (h) show conventional reflectometer heterodyne phase trace and its spectrum, and (i) and (j) show Doppler shift deduced from center of gravity and its spectrum.

6(g) and (h) show time traces of the conventional reflectometer heterodyne phase and its wavelet spectrum, respectively. Since conventional reflecometry changes the probing frequency with 10 ms, the time window of the conditional averaging is different. Here 14 burst events are detected and averaged. Figure 6(g) shows that the phase jumps before the bursts starts. Weak but finite 100 kHz fluctuations are observed during the bursts, as shown in Fig. 6(h). Here, the 100 kHz fluctuations are identical to the WCM, and its also appears without bursts, i.e. during the waiting time between two bursts. Note that the GAlf and the WCM have similar frequencies, around 100 kHz, but the GAlf is a magnetic fluctuation while the WCM is a density fluctuation [12]. These two fluctuations are stationary in I-mode. Figure 6(i) and (j) show the Doppler shift frequency fluctuation and its spectrum estimated by the center of gravity of the spectrum. Center of gravity of the spctrum is defined as, $f_d = \int f P(f) df / \int P(f) df$, where $P(f)$ is a power spectrum of IQ signals, which is obtained by heterodyne system. Here the center of gravity is calculated by FFT for 2.5 τs time window, and is shifted 0.5 τs for overlapping. The Doppler shift starts to increase before the bursts, as shown in Fig. 6(i). Fluctuations around 100 kHz are also detected, as shown in Fig. 6(j). However, here the 100 kHz fluctuations are possibly produced by the result of turbulence

amplitude modulation. Thus, it is doubtful to claim an existence of 100 kHz fluctuations in velocity fluctuations. The detected 100 kHz fluctuations in velocity fluctuations are also discussed below.

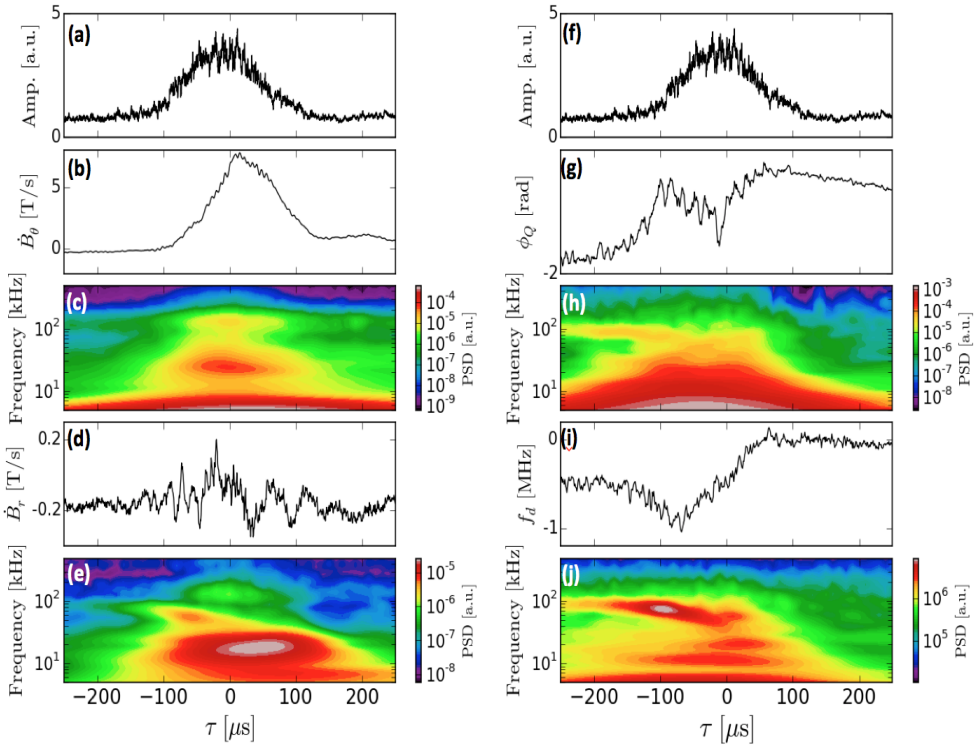

Figure 7. Dynamics of conditional averaged signals and their wavelet spectra in late I-phase in the same representation as figure 6.

For late I-phase, a template method [15], which is useful to detect quasi-periodic nonlinear waves, is performed to poloidal magnetic field signals. 50 events are extracted from discharge #29818 of 4.00-4.10 s. Figure 7 is the same representation as figure 6. From figure 7(c), 100 kHz magnetic fluctuations are observed during the bursts, however, it is not stationary like late I-mode. In figure 7(e), 100 kHz magnetic fluctuations are also observed only during the bursts. In addition, around 90 kHz fluctuations are detected before the bursts. Here the fluctuations may be a precursor [7]. Clear precursors at a frequency around 90 kHz are also observed in density fluctuations, as shown in Fig. 7(h). Here, conventional reflectometer probing frequency is also changed in 10 ms, thus conditional averaging is performed for 15 events. A precursor seems to be detected in velocity fluctuations at around 90 kHz, as shown in Fig. 7(j). Since velocity fluctuations are determined by the center of gravity, careful attention is needed. We will discuss about this precursor like mode in next paragraph. It is interesting to note that velocity fluctuations at around 10 kHz are observed during the bursts, as shown in Fig. 7(j). The identification of this mode is for future work.

In figure 6 and 7, velocity fluctuations are deduced from a center of gravity. Sometimes, the center of gravity provides only misleading information about velocity

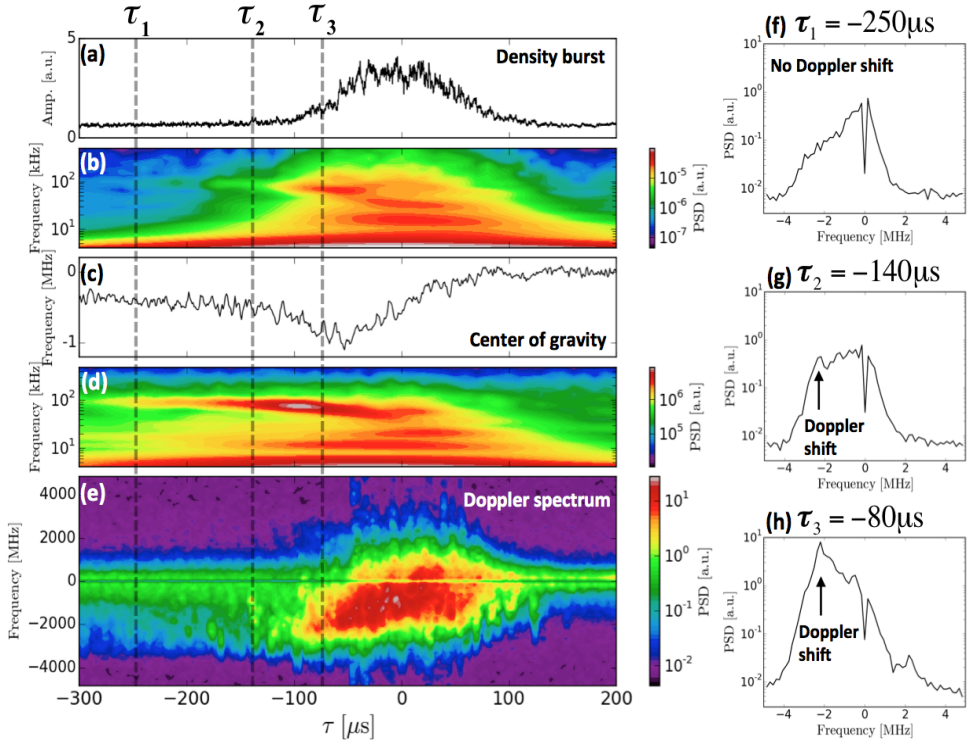

Figure 8. Conditional averaged (a) density bursts and (b) its spectrum, (c) velocity fluctuations deduced from center of gravity and (d) its spectrum, and (e) Doppler spectrum. Conditional averaged are performed with same discharge/time window as figure 7. Doppler spectra in several times are shown in (f), (g) and (h).

fluctuations since asymmetric components in the spectrum, which are not directly related to a Doppler shift, can change the center of mass. Therefore, the confirmation of the Doppler shift in the spectrum is necessary. Figure 8(e) shows the conditionally averaged Doppler spectrum in late I-phase. Time evolutions of the Doppler spectrum are obtained by FFT for 6.4 τs time windows (64 points for 1 μs time resolutions) with 2.5 μs shift for overlapping. Discharges and the number of averaged burst events are the same as in figure 7. Conditional averaged density bursts and its wavelet spectrum, and conditional averaged velocity fluctuations determined by center of gravity and its wavelet spectrum, are also shown in Fig. 8(a)-(d), respectively. Before the onset of the bursts, at $\tau_1 = -250\,\mu$s, the Doppler shift deduced from the center of gravity and 90 kHz fluctuations are detected, as shown in Fig. 8(c) and (d). In this time τ_1, the turbulence amplitude is low and no 90 kHz fluctuations, i.e. amplitude modulations, are observed, as shown in Fig. 8(a) and (b). The Doppler spectrum shows the absence of the Doppler shift, as shown in Fig. 8(f). Therefore, here the 90 kHz fluctuations, which are obtained from center of gravity, are false signals and not velocity fluctuations. In Fig. 8(b), 90 kHz fluctuations start to be observed in the turbulence amplitude spectrum at $\tau_2 = -140\,\mu$s, as precursor. In this time τ_2, weak Doppler shift is observed, as shown in Fig. 8(g). Then in time $\tau_3 = -80\,\mu$s, sufficient amplitude level (Fig. 8(a))

and strong Doppler shift (Fig. 8(h)) is detected. However, there are still some problems to decide that 90 kHz fluctuations exist in velocity fluctuations, as mentioned in the following; (i) the Doppler shift $f_D(t) = u_\perp(t)k_\perp(t)/2\pi$ is understood as a combination of velocity fluctuations $u_\perp(t)$, and wave number fluctuations $k_\perp(t) = 2k_i\sin\theta(t)$ (k_i is an incident wave number). Therefore, to distinguish between velocity and wave number fluctuations is difficult in principle [16]. (ii) The turbulence amplitude, i.e. density bursts, is modulated in 90 kHz, as shown in Fig. 8(b). Therefore, this Doppler shift could be a result of amplitude modulations. From these reasons, it is difficult to claim the existence of 90 kHz velocity fluctuations in late I-phase.

Next, the time scales of bursts in late I-phase and late I-mode are calculated. Figure 9(a) shows a conditionally averaged waveform of the density bursts in late I-mode. The duration of the bursts τ_{dur} is obtained from this waveform. An estimation results in $\tau_{dur} \sim 9\,\mu$s in late I-mode and $\tau_{dur} \sim 200\,\mu$s in late I-phase, respectively. The duration of the density bursts is much different. Rise and decay times are also estimated by the derivative of the conditional averaged waveform with time, as shown in Fig. 9(b). Rise time τ_{rise} and decay time τ_{decay} are obtained as $\tau_{rise} \sim 4\,\mu$s and $\tau_{decay} \sim 4\,\mu$s in late I-mode and $\tau_{rise} \sim 40\,\mu$s and $\tau_{decay} \sim 60\,\mu$s in late I-phase, respectively. The rise and decay time of the density bursts in late I-mode are shorter than in late I-phase. The time scales of poloidal magnetic field fluctuations are also estimated. In late I-mode, $\tau_{dur} \sim 120\,\mu$s, $\tau_{rise} \sim 40\,\mu$s and $\tau_{decay} \sim 60\,\mu$s are obtained. Compared to the time scales of the density bursts, magnetic fluctuations are slowly changing. While in late I-phase, $\tau_{dur} \sim 210\,\mu$s, $\tau_{rise} \sim 80\,\mu$s and $\tau_{decay} \sim 100\,\mu$s are deduced, which are almost same time scales with the density bursts time scales. These results suggest that density bursts in late I-phase are more connected with magnetic activities.

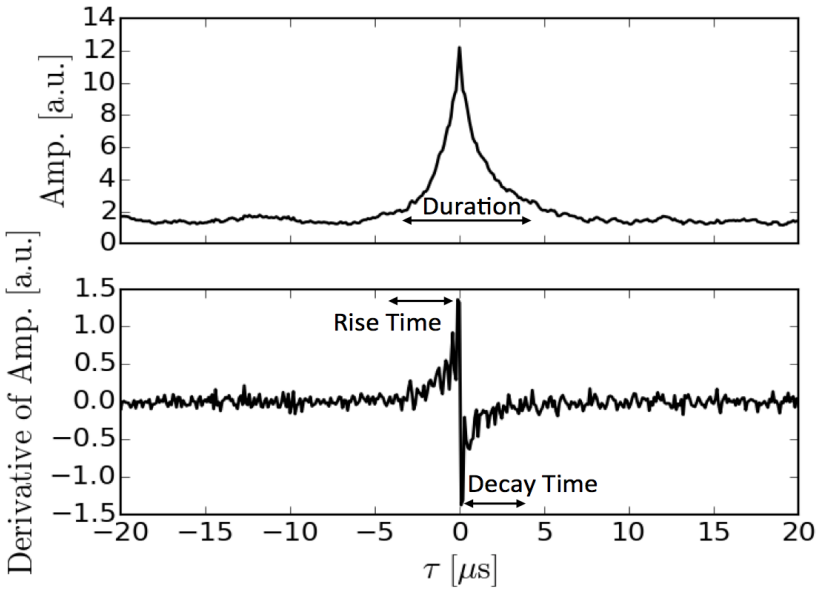

Figure 9. (a) Conditional averaged density bursts and (b) its time derivation in late I-mode. Duration, rise time and decay time are shown in the graph.

Intermittency of the bursts is also investigated. Figure 10 shows the probability distribution function (PDF) of density bursts period. The bursts intermittently occur in 10 μs to 1 ms periods in late I-mode discharge #29744 at 2.40-2.44 s, as shown in black line. In late I-phase, intermittency is different in different discharges. The PDF of the discharge #29818 at 4.00-4.10 s seems to be accumulated at around 1.8 ms, as shown in red line. While the PDF of the discharge #30609 at 5.40-5.50 s is randomly observed. These results suggest that late I-mode bursts are intermittently while late I-phase bursts are sometimes periodic and sometimes intermittent.

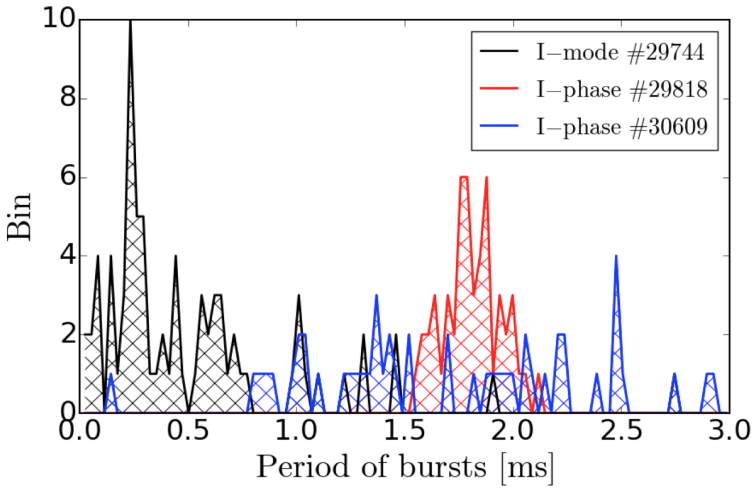

Figure 10. Density bursts period are calculated as PDF. PDF of late I-mode discharge #29744 is shown as black line. PDFs of late I-phase are shown with two different discharges, #29818 with red line and #30609 with blue line. Late I-phase intermittency is different in different discharges.

5. summary

Late I-mode and late I-phase density bursts and turbulence are compared by using Doppler reflectometry. Conditional averaging is performed to quantify turbulence, time scales of bursts and intermittency of bursts. The most prominent similarity between late I-mode and late I-phase might be an existence of precursors before the density bursts. The precursor frequencies are around 100 kHz in late I-mode and around 90 kHz in late I-phase, respectively. In late I-mode, this precursor might be connected with WCM, which frequency is also 100 kHz. Differences are as follows; (i) In late I-mode, 100 kHz fluctuations (i.e. WCM/GAlf) become strong during the bursts, however, they appear statistically likewise in the phase between two bursts. However, in late I-phase, 90 kHz fluctuations are observed only before the bursts, i.e., only appear as precursors. (ii) The time scale of the density bursts is much different. In late I-mode, density bursts and magnetic fluctuations time scales are one order different, while in late I-phase, density

bursts and magnetic fluctuations time scales are of the same order. (iii) In late I-mode, the bursts appear intermittently, while in late I-phase, the bursts occurs sometimes periodically and sometimes intermittently, depending on discharges. During the bursts, low frequency modes in velocity fluctuations are also observed in late I-phase. The identification of this mode is left for future work.

Acknowledgments

We thank the turbulence meeting group members for fruitful discussions. This work was supported by JSPS Research Fellow (JP4J00560).

References

[1] D.G. Whyte *et al., Nucl. Fusion* **50**, 105005 (2010)
[2] F. Ryter *et al., Nucl. Fusion* **57**, 016004 (2017)
[3] T. Happel *et al., Nucl. Fusion* **56**, 064004 (2016)
[4] T. Happel *et al., Plasma Phys. Control. Fusion* **59**, 014004 (2017)
[5] S.-I. Itoh *et al., Phys. Rev. Lett.* **67**, 2485 (1991)
[6] G.D. Conway *et al., Phys. Rev. Lett.* **106**, 065001 (2011)
[7] G. Birkenmeier *et al., Nucl. Fusion* **56**, 086009 (2016)
[8] P. Manz *et al., Nucl. Fusion, To be published.*
[9] H. Biglari *et al., Phys. Fluids B* **2**, 1 (1990)
[10] P.H. Diamond *et al., Plamsa Phys. Control. Fusion* **47**, R31 (2005)
[11] ITER physics basis, *Nucl. Fusion* **39**, 2137 (1999)
[12] P. Manz *et al., Nucl. Fusion* **55**, 083004 (2015)
[13] M. Hirsch *et al., Plasma Phys. Control. Fusion* **43**, 1641 (2001)
[14] H. Johnsen *et al., Phys. Fluids* **30**, 2239 (1987)
[15] S. Inagaki *et al., Plasma Fusion Res.* **9**, 1201016 (2014)
[16] T. Estrada *et al., Nucl. Fusion* **52**, 082002 (2012)